# Surfactant-Free CuInS$_2$ Nanocrystals: An Alternative Counter-Electrode Material for Dye-Sensitized Solar Cells

Rong-Yue Yao,[†] Zheng-Ji Zhou,[†] Ze-Liang Hou, Xia Wang, Wen-Hui Zhou, and Si-Xin Wu*

The Key Laboratory for Special Functional Materials of MOE, Henan University, Kaifeng 475004, China

ABSTRACT: Surfactant-free CuInS$_2$ (CIS) nanocrystals (NCs) were synthesized by replacing organic capping ligands with inorganic ions S^{2-}. The efficacy of ligand exchange was probed by thermogravimetric analysis (TGA), scanning electron microscopy (SEM), transmission electron microscopy (TEM), X-ray diffraction (XRD), UV−vis spectroscopy, and Fourier-transform infrared (FTIR). The surfactant-free CIS NCs films were obtained by drop-casting onto the clean FTO glass. The electrical conductivity and electrocatalytic activity of CIS NCs films were sharply increased due to the improved interparticle coupling after ligand exchange. When the surfactant-free CIS films were used as counter electrode (CE) in dye-sensitized solar cells (DSSCs), a conversion efficiency of η = 5.77% was achieved without sintering.

KEYWORDS: CuInS$_2$ nanocrystals, counter electrode (CE), conversion efficiency (η), dye-sensitized solar cells (DSSCs), ligand exchange
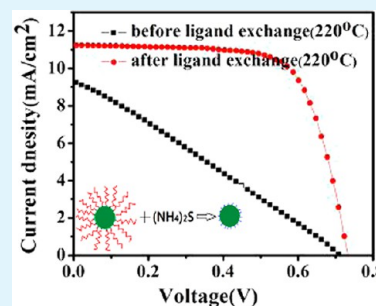
1. INTRODUCTION

Dye-sensitized solar cells are promising candidates for low-cost and clean energy conversion devices.[1−3] In general, it comprises a dye-adsorbed TiO$_2$ photoanode, a counter electrode (CE), and an electrolyte with a redox couple (I$^-$/I$_3^-$). One of the most important components in DSSCs is the CE, which collects electrons from external circuit and catalyzes the reduction of triiodide ions in electrolyte. The CEs in DSSCs are usually made of the noble metal Pt due to its superior electrocatalytic activity, high electrical conductivity, and good stability.[4] However, the scarcity and expensiveness of platinum limit its potential applications in DSSCs, so it is highly urgent to find alternative low-cost CE materials with relatively high catalytic activity for DSSCs.[5] Nowadays, various materials such as carbon-based materials,[6−8] conducting polymers,[9,10] and inorganic semiconductor materials[11−14] have been investigated as alternatives in DSSCs. Among them, inorganic semiconductor materials possess the advantage of both facile preparation and diversity of materials. Especially, metal sulfides have drawn enormous attention. Many transition metal sulfides, such as NiS,[15] CoS,[16,17] MoS$_2$,[18] PbS,[19,20] etc, have been exploited as effective CE materials. Recently, ternary or quaternary sulfides[12,21] were studied as CE in DSSCs. CuInS$_2$ (CIS) is well-known as one of the most promising photovoltaic (PV) materials, and it is widely used in thin-film solar cells.[22,23] Recently, CIS film was reported as CE in DSSCs which exhibits high power conversion efficiency.[24] In order to obtain high-quality, monodispersed nanocrystals (NCs), the CIS NCs were capped by DDT organic molecules for prevention of aggregation and for size and shape control of CIS NCs. The presence of these large organic molecules resulted in highly insulating barriers which blocked the electronic transfer between NCs in CIS films, limiting the performance of electronic and optoelectronic devices. Although high temper-ature annealing can remove a part of the organic molecules whereas the defects will leave simultaneously,[25,26] the residual organic compounds are carbonized after burning in inert gases. As we know, an ideal CE must possess high conductivity and good catalysis; however, it is usually not easy to meet both above requirements simultaneously for inorganic semiconductor materials. In order to improve both electrical conductivity and superior electrocatalytic activity of CIS NCs films, we tried to fabricate the organic-free CIS NCs by a ligand exchange method. Surfactant-free CIS NC films facilitate to expose the active surface; meanwhile, the removal of organic molecules in CIS NC films dramatically improved inter-NC charge trans-port.[27,28]

In this paper, we report a novel method to obtain surfactant-free CIS NC films as the CE in DSSCs through removing bulky surfactant ligands from DDT-capped CIS NCs. The results of Fourier-transform infrared (FTIR) spectra and thermogravi-metric analysis (TGA) characterization demonstrated that the organic molecules on the surfaces of CIS NCs can be successfully removed by ligand exchange. The measurement of electrical properties illuminated that the conductivity was highly enhanced for surfactant-free CIS NCs due to the absence of organic molecules. The excellent performance of DSSCs using surfactant-free CIS NC films as CE can be obtained without annealing treatment.
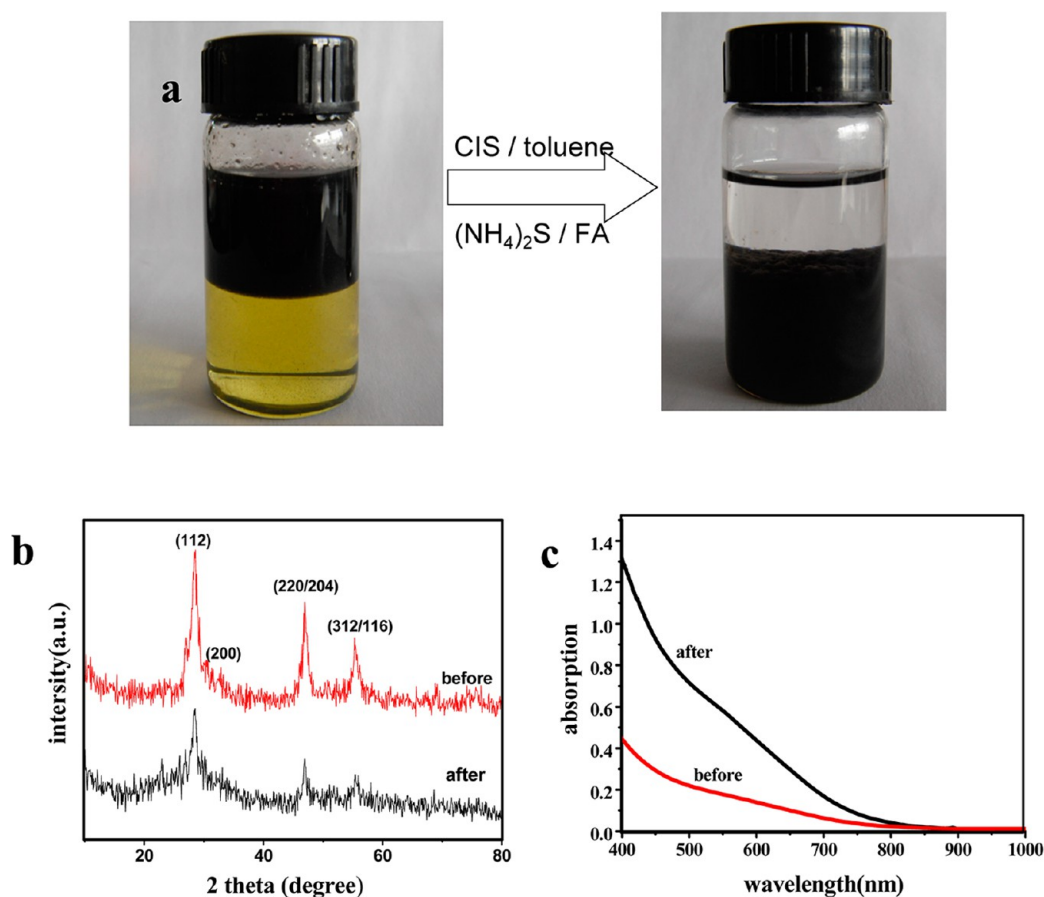
2. EXPERIMENTAL SECTION

2.1. Synthesis of CuInS$_2$ Nanoparticles. In a typical synthesis of CIS NCs, indium acetate (58.2 mg, 0.2 mmol), with copper(I) chloride (19.8 mg, 0.2 mmol), 1-dodecanethiol (DDT, 0.5 mL), and

Figure 1. (a) Black colored colloidal dispersion of CIS NCs undergoes the phase transfer from toluene to formamide (FA) upon exchange of the original organic surface ligands with S^{2-}. (b) Powder XRD patterns of CIS NCs before (red) and after (black) ligand removal. (c) Optical absorption spectra of CIS NCs before (red) and after (black) ligand removal.

ODE (~5 mL) were mixed in a three-necked flask. The mixture was continuously degassed for 5 min and filled with argon three times. Then, the solution was heated to 100 °C and kept for 10 min until a clear solution was formed. After that, the solution was heated up to 240 °C and kept for 1 h. During the temperature increasing, the color of the solution progressively changed from colorless to green, yellow, red, and finally black. Subsequently, the solution was removed from the heater and cooled at room temperature. The precipitates were separated by centrifugation, washed with hexane and acetone for three to five times, and dried at vacuum box.

2.2. Ligand Exchange. Colloidal dispersions of CIS NCs with organic ligands were prepared in nonpolar solvents hexane, while solutions of inorganic ligands were prepared in polar formamide (FA) immiscible with hexane. For a typical ligand exchange using S^{2-} ions, 10 mL of CIS NCs solution (2 mg/mL) was mixed with 10 mL of $(NH_4)_2S$ solution (20 mL/mL). The mixture was stirred for about 2 h leading to a complete phase transfer of CIS NCs from hexane to the FA phase. The phase transfer can be easily monitored by the color change of hexane (black to colorless) and FA (yellow to black) molecules. The FA phase was separated out followed by triple washing with ethanol to remove any remaining nonpolar organic species.

2.3. CIS Thin Film Deposition and DSSCs Fabrication. Twenty mg of CIS NCs was dispersed in 1 mL of solvent (toluene for the DDT-capped CIS NCs and deionized water for the surfactant-free CIS NCs, respectively) and sonicated for 10 min to form a uniform nanoparticle "ink". The "ink" was then drop-casted onto the clean FTO glass substrate. The drop-casted area was controlled to be the same, and the thickness of CIS was adjusted by the drop volume of "ink". The films were fully dried by drying at 220 °C for 30 min or annealed at 500 °C for 20 min under the protection of argon to obtain CIS NC films as CE.

The TiO$_2$ photoanodes with the effective area of 0.6 × 0.6 cm^2 were immersed overnight in 0.3 mM ethanolic solution of dye N-719 (Solaronix) at room temperature, then taken out and rinsed with ethanol to remove excess dye adsorbed, and dried in air at room temperature. The sandwich-type solar cell was assembled by placing the CIS CE on the N-719 dye-sensitized photoelectrode and clipped together as an open cell for measurements. The cell was then filled with a liquid electrolyte composed of 0.1 M anhydrous LiI, 0.12 M I$_2$, 1.0 M DMPII, and 0.5 M tert-butylpyridine in dehydrated acetonitrile by capillary force.

2.4. Characterization. The particles size and morphology of the products were investigated using a scanning electronic microscope (SEM, JSM-5600LV at 20 KV) and transmission electron microscopy (TEM, JSM-2010 at 200 KV). The crystal structure was determined by X-ray diffraction (XRD, Philips X' PertPro; Cu Kα: $\lambda = 0.154056$ nm). UV−vis absorption spectra of NC dispersions were recorded using UV−vis spectroscopy (Lambda 35, Perkinelmer); Fourier-transform infrared (FTIR) spectra were acquired in the transmission mode using a Nicolet Nexus-670 FTIR spectrometer. Thermogravimetric analyses (TGA) was carried out under nitrogen flow (300 cm^3/min) at a heating rate of 5 °C/min using a TG/DTA 6200 thermogravimetric analyzer, SII, Inc.

The photocurrent−voltage (J−V) measurements were taken on a digital source meter (Keithley 2400, computer-controlled) with the device under AM 1.5 G spectra, which was produced by a solar simulator (Newport, Oriel class A, SP91160A, USA). The light power density was calibrated against a Si-based reference cell (Hamamatsu S1133) to accurately simulate the full-sun intensity (100 mW cm^{-2}). Cyclic voltammetry (CV) was carried out in a three-electrode system in an acetonitrile solution of 0.1 M LiClO$_4$, 10 mM LiI, and 1 mM I$_2$ at a scan rate of 50 mVs^{-1}. Platinum served as a counter electrode, and

3144

dx.doi.org/10.1021/am400031w | *ACS Appl. Mater. Interfaces* 2013, 5, 3143−3148

the Ag/Ag+ couple was used as a reference electrode. Electrochemical impedance spectroscopy (EIS) was performed in the dark using an impedance measurement unit (ZAHNER-elektrik IM6) in the frequency range of $0.1-10^5$ Hz with ac amplitude of 10 mV and an applied bias voltage of 0.8 V between the CE and the working electrode.

3. RESULTS AND DISCUSSION

For a typical ligand exchange procedure, we combined solutions of organic-capped NCs in a nonpolar solvent (toluene) with the solution of inorganic ligands $(NH_4)_2S$ in formamide (FA). The two-phase mixture containing immiscible layers of FA and nonpolar solvent was stirred for about 2 h, and complete transfer of NCs from toluene solvent to FA was observed (Figure1a). The XRD patterns of CIS NCs before and after ligand exchange were showed in Figure1b. The peak positions can be indexed to those of chalcopyrite $CuInS_2$ (JCPDS No. 38-777). The major XRD diffraction peaks appeared at 2θ = 28.39°, 46.95°, and 55.44° attributed to (112), (204)/(220), and (110)/(312), respectively. The sizes of CIS NCs before and after ligand exchange were calculated about 7.6 and 6.9 nm, respectively. From the results of XRD, it was demonstrated that ligand exchange distinctly changes the distribution and crystal of CIS NCs. Figure 1c demonstrated the optical absorption spectra of CIS nanoparticles dispersed in tetracarp (before ligand exchange) and ethanol (after ligand exchange), the result shows a broad absorption in the visible region. After ligand exchange, the absorption of surfactant-free CIS NCs is notably stronger than that of DDT-capped CIS NCs, especially in the visible light range from 400 to 700 nm. The similar results were also reported in PbS[29] and CdSe[27] systems. The reason resulted from the quantum mechanical coupling energy due to the CIS nanoparticles being more close in proximity to each other after the removal of the insulating surfactant ligands.

In order to confirm whether the organic molecules on the CIS NCs were completely removed by ligand exchange, Figure 2 shows FTIR spectra of CIS NCs before and after the ligand
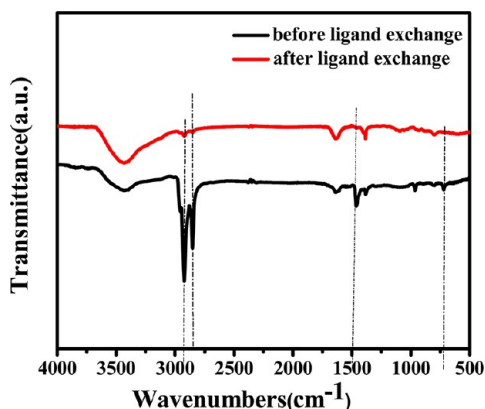

Figure 2. FTIR spectra of CIS NCs before (black) and after (red) ligand exchange.

exchange. From Figure 2, it is clear that, after ligand exchange, the transfer of CIS NCs from toluene to FA resulted in the complete disappearance of the following bands: bands at 2852 and 2925 cm^{-1} corresponding to C−H stretching in the original organic ligands; the band at 1465 cm^{-1} corresponding to deformation vibration of −CH$_2$; the band at 721 cm^{-1} corresponding to the rocking vibration peak when there is more

than four ethylenes in an organic molecule. These results confirm the efficacy of S^{2-} ligands in complete removal of the organic ligands, forming surfactant-free colloidal NCs.

The TEM images of the DDT-capped and surfactant-free CIS NCs are shown in Figure 3, we can observe that the size
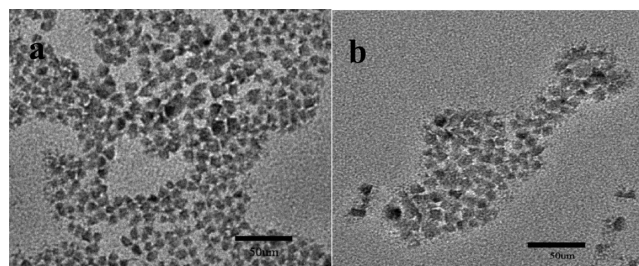
Figure 3. TEM image of CIS NC films before (a) and after (b) ligand exchange.

and shape of CIS NCs are still retained by ligand exchange. However, there are some agglomerations after ligand exchange due to the removal of organic long chains on the surface of NCs.

Figure 4 shows that the total weight loss of the surfactant-free CIS NCs (10%) is much lower than that of the DDT-
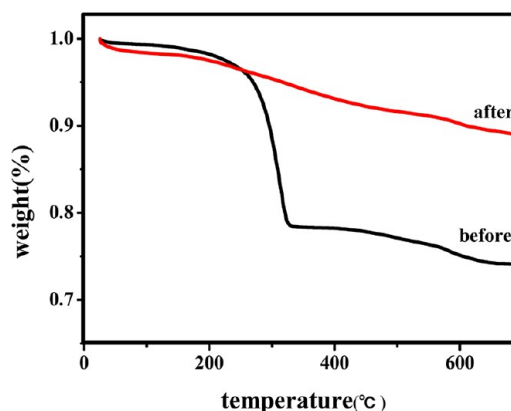

Figure 4. TGA scans of CIS NCs before (black) and after (red) ligand exchange.

capped CIS NCs (28%). For DDT-capped CIS NCs, a sharp weight loss occurs in about 300 °C; then, there is a slow weight loss between 325 and 700 °C. The DTA curve has a large exothermic peak at 275 °C which is attributed to the decomposition of DDT. After ligand exchange, the total weight loss of the surfactant-free CIS NCs is lower than that of DDT-capped CIS NCs due to the absence of organic surfactant.

The top-view and cross-sectional SEM images of the CIS NC thin films are presented in Figure 5. All films showed near uniformity and were free of cracks, which are important properties for solar cell device fabrication. For the DDT-capped CIS NC films (Figure 5a,b), organic moieties remained in CIS films because organic capping ligands (1-dodecanethiol in this case) were used for dispersion of CIS NCs. To remove organic moieties as much as possible, an annealing process was carried out at 500 °C under Ar atmosphere; we can observe from Figure 5c,d that organic moieties were removed, and at the same time, there existed a small amount of cracks. The thickness of CIS NC film annealed at 500 °C was a little decreased from 2.0 μm to about 1.9 μm due to the removal of
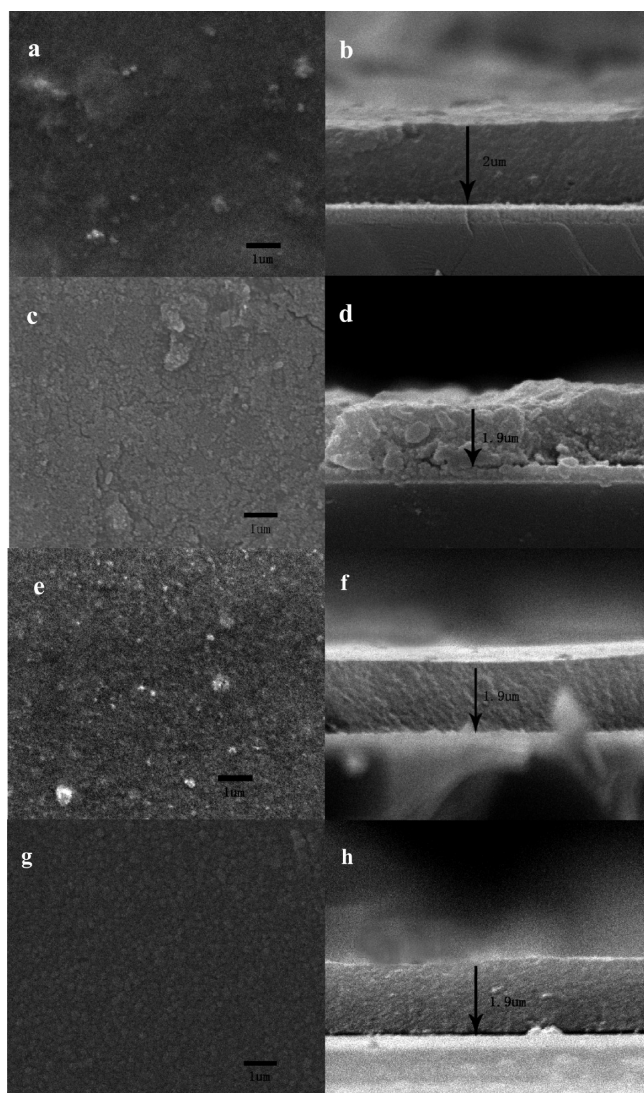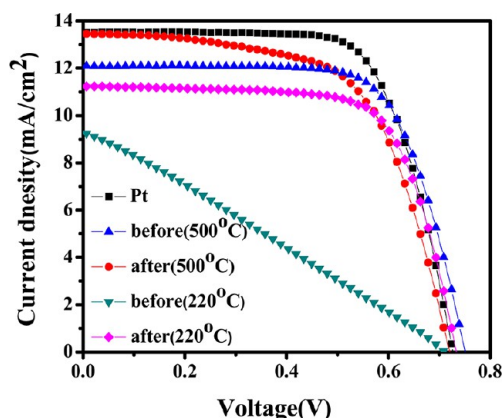
Figure 5. SEM image of CIS NC films before [(a, b, dried at 220 °C) (c, d, annealed at 500 °C)] and after ligand removal [(e, f, dried at 220 °C) (g, h, annealed at 500 °C)].

Figure 6. $J-V$ characteristics of DSSCs with CIS CEs and Pt CE.

organic molecules. In the surfactant-free CIS NC films shown in Figure 5e,f, the grains in the CIS film were more clearly seen. The thickness of surfactant-free CIS NC films was about 1.9 μm for drying at 220 °C and annealing at 500 °C, respectively. The thickness of the films were kept constant even if annealing at 500 °C.

In order to investigate whether the conductivity was highly enhanced with ligand exchange, we use the CIS NC films as the CE in DSSCs and check the effect of the ligand exchange and annealing on the performance of DSSC devices. Figure 6 shows the photovoltaic performance of DSSCs based on the various CIS films as CE materials. The detailed photovoltaic parameters, such as short-circuit photocurrent (J_{sc}), open-circuit voltage (V_{oc}), fill factor (FF), and efficiency (η) are summarized in Table1. From Figure 6 and Table 1, evidently, we can find that, when the DDT-capped CIS NC films dried at 220 °C, the photovoltaic performance of DSSCs was very poor (only 1.78%), since the data of photovoltaic parameters, such as J_{sc}, V_{oc}, and FF were very low (9.25, 0.36, and 27.35, respectively). For the surfactant-free CIS NC films dried at 220 °C, the photovoltaic performance of DSSCs was highly

enhanced to 5.77%. The high performance of DSSCs resulted from the improved photovoltaic parameters, such as J_{sc}, V_{oc}, and FF (11.25, 0.73, and 70.04, respectively). Since the thickness of the CIS films before and after ligand exchange was nearly the same, the difference of photovoltaic performance of DSSCs was mainly caused by quality of the CIS films. Because of the existence of organic molecules on the DDT-capped CIS NCs, the electrical transfer between the CIS NCs was seriously hindered, with the photocurrent density obviously lower (9.25 mA/cm^{-2}). At the same time, after ligand exchange, the photocurrent density was enhanced (11.25 mA/cm^{-2}) due to the removal of organic molecules on the surfaces of CIS NCs.

When the DDT-capped CIS films was annealed at 500 °C for 20 min, we can observe that the photovoltaic performance of DSSCs was highly improved from 1.78% to 5.97%; besides the dense CIS films, the removal of organic molecules on the surfaces of CIS NCs was a crucial factor. Another interesting result can also been found. When the organic molecules on the surfaces of CIS NCs were removed, even if the surfactant-free CIS films was dried at 220 °C, the photovoltaic performance of DSSCs still was very high (5.77%); the conversion efficiency of DSSCs was 6.35% when the surfactant-free CIS films was annealed at 500 °C for 20 min. The conversion efficiency of DSSCs was just increased about 10%. For the consideration of cost reductions, it is not necessary to heat treat when the CIS films were prepared by ligand exchanges.

Usually, if the NC films were used as CE in DSSCs, in order to improve the performance of devices, the annealing process is necessary to remove the organic molecules.[13] The annealing process will result in the growth of small NCs, thus decreasing the surface area of NC films. Moreover, annealing in inert gas, parts of organic compounds will be carbonized.[26] Here, through ligand exchange, the surfactant-free CIS NC films possess not only the large surface area but also the high conductivity; therefore, surfactant-free CIS NC films simultaneously satisfy the requirement of the ideal CE in the DSSC device.

EIS measurement was conducted to analyze the electrochemical characteristics of the different CE toward iodide couple electrolyte. It can be seen that the Nyquist plots shown in Figure 7 includes several regions from the high frequency regions to the low frequency regions representing various resistances: (i) ohmic serial resistance (R_s), representing the outside circuit resistance (substrates resistance and lead connections); (ii) charge transfer resistance (R_{ct}), corresponding to the electron transfer ability at the electrode/electrolyte interface.

**Table 1. Photovoltaic Performance of DSSCs with Different Thicknesses of CIS CEs and Pt CE**

material	J_{SC} (mA/cm^{-2})	V_{OC} (V)	FF	η (%)	R_s (Ω)	R_{ct} (Ω)
Pt	13.52	0.72	70.00	6.87	14.08	1.61
before ligand exchange						
CIS (500 °C, 20 min)	13.45	0.72	61.69	5.97	14.88	2.55
CIS (220 °C, 30 min)	9.25	0.36	27.35	1.78	14.45	3.98
after ligand exchange						
CIS (500 °C, 20 min)	12.08	0.75	70.10	6.35	14.91	2.54
CIS (220 °C, 30 min)	11.25	0.73	70.04	5.77	14.69	2.63
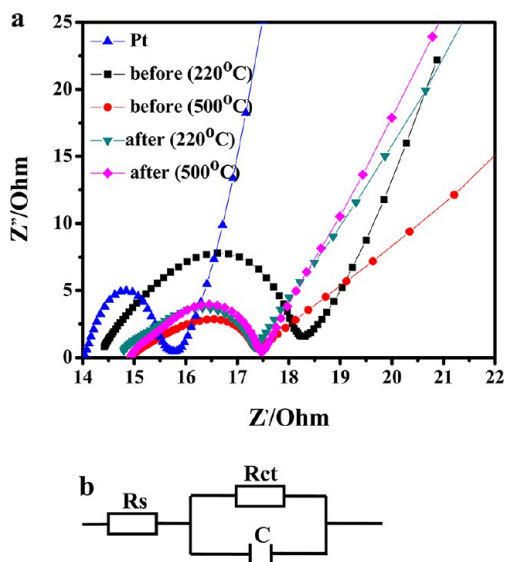
Figure 7. Equivalent circuit and Nyquist plots (a) and the equivalent circuit (b) of the symmetric cells with two identical CEs of CIS before and after ligand exchange (dried at 220 °C). R_s: Ohmic serial resistance. R_{ct}: charge-transfer resistance of single electrode. C: double layer capacitance.

The values of R_s and R_{ct} obtained by fitting the spectra in Figure 7 and an EIS spectrum analyzer are summarized in Table 1. The high-frequency intercept on the real axis represents the series reistance (R_s); the semicircle in the high-frequency range results from the charge-transfer resistance (R_{ct}). When the CEs have nearly the same absolute R_s, the effect of various CEs caused by R_s on the photovoltaic performance can be omitted.

For the DDT-capped CIS NC films, after annealing at 500 °C for 20 min, the R_{ct} was obviously decreased from 3.98 to 2.55 Ω, and the R_{ct} (2.63Ω) of the surfactant-free CIS NC films (dried at 220 °C) was lower than that of DDT-capped CIS NC films, which indicated a superior catalytic performance of surfactant-free CIS NC films. The annealing process did not obviously impact the R_{ct} for the surfactant-free CIS NC films, and the annealing process did not clearly improve the conductivity.[30]

Figure 8 shows cyclic voltammograms for the reduction of I_2/I_3^- obtained at the various electrode materials in the acetonitrile solution containing 0.1 M LiClO$_4$, 0.45 mM LiI, and 0.05 mM I$_2$ at a scan rate of 50 mVs^{-1}. The peak currents and the peak-to-peak separation (Epp), which is negatively correlated with the standard electrochemical rate constant of a redox reaction, are two important parameters for comparing catalytic activities of different CEs. The higher peak current densities and lower Epp value reveal that it is a remarkable electrochemical catalyst for the reduction of I_3^-.[31,32] Two pairs of redox peaks were assigned to the following reactions:[33,34]
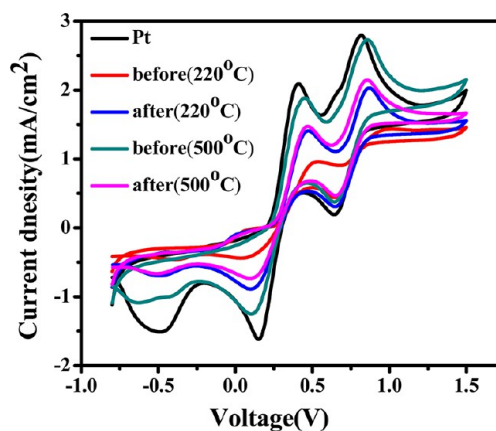
Figure 8. Cyclic voltammograms obtained at a scan rate of 50 mV s^{-1} for the reduction of I_2/I_3^- at the various electrode materials.

$$I_3^- + 2e \rightleftharpoons 3I^- \tag{1}$$

$$3I_2 + 2e \rightleftharpoons 2I_3^- \tag{2}$$
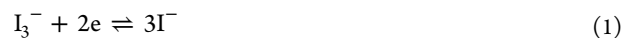
The peak positions of the CV curve for the surfactant-free CIS electrode are very similar to the Pt electrode, illuminating that CIS electrode after ligand exchange has a similar electrocatalytic function for the redox reaction to Pt electrode. Furthermore, the after ligand exchange CIS electrode exhibits a higher current density, as can be seen from the large peak area[13] in the CV curve, suggesting a larger electrode active surface.

It is expected that a significant improvement in device performance could be achieved by optimizing the thickness of surfactant-free CIS films and the methods of film formation (such as, spin coating and drop casting, etc), and in a previous report about CE materials, the thickness of CE films affected the performance of DSSCs obviously.[12,35] For example, The high efficiency DSSC reported by Cui et al. has a thickness of CIS CE about 13 μm.[23] Further works in these topics are in progress in our lab.

4. CONCLUSIONS

In summary, we have demonstrated a novel Pt-free CE for DSSCs based on low-cost CIS with a simple one-pot route synthesis; the organic ligands can be easily removed by ligand exchange. The results demonstrate that surfactant removal improves its optoelectronic properties and represents a promising strategy for integration of nanocrystal in electronic and optoelectronic devices.

■ AUTHOR INFORMATION

Corresponding Author

*E-mail: wusixin@henu.edu.cn.

Author Contributions

[†]R.Y. and Z.Z. contributed equally to this work.

Notes

The authors declare no competing financial interest.

■ REFERENCES

(1) Regan, B. O.; Grätzel, M. *Nature* **1991**, *353*, 737−740.

(2) Hagfeldt, A.; Boschloo, G.; Sun, L. C.; Kloo, L.; Pettersson, H. *Chem. Rev.* **2010**, *110*, 6595−6663.

(3) Zhen, F.; Eshbaugh, A.; Schanze, K. S. *J. Am. Chem. Soc.* **2011**, *133*, 3063−3069.

(4) Papageorgiou, N.; Maier, W. F.; Grätzel, M. *J. Electrochem. Soc.* **1997**, *144*, 876−884.

(5) Wu, M. X.; Lin, X.; Hagfeldt, A.; Ma, T. L. *Angew. Chem., Int. Ed.* **2011**, *50*, 3520−3524.

(6) Li, K. X.; Luo, Y. H.; Yu, Z. X; Deng, M. H.; Li, D. M.; Meng, Q. B. *Electrochem. Commun.* **2009**, *11*, 1346−1349.

(7) Dong, P.; Pint, C. L.; Hainey, M.; Mirri, F.; Zhan, Y. J.; Zhang, J.; Pasquali, M.; Hauge, R. H.; Verduzco, R.; Jiang, M.; Lin, H.; Lou, J. *ACS Appl. Mater. Interfaces* **2011**, *3*, 3157−3161.

(8) Malara, F.; Manca, F.; Marco, L. D.; Pareo, P.; Gigli, G. *ACS Appl. Mater. Interfaces* **2011**, *3*, 3625−3632.

(9) Trevisan, R.; Döbbelin, M.; Boix, P. P.; Barea, E. M.; Tena-Zaera, R.; Mora-Seró, I.; Bisquert, J. *Adv. Energy Mater.* **2011**, *1*, 781−1784.

(10) Cho, S. H.; Hwang, S. H.; Kim, C.; Jang, K. *J. Mater. Chem.* **2012**, *22*, 12164−12171.

(11) Huang, X. M.; Huang, S. Q.; Zhang, Q. X.; Guo, X. Z.; Li, D. M.; Luo, Y. H.; Shen, Q.; Toyoda, T.; Meng, Q. B. *Chem. Commun.* **2011**, *47*, 2664−2666.

(12) Xin, X. K.; He, M.; Han, W.; Jung, J.; Lin, Z. Q. *Angew. Chem., Int. Ed.* **2011**, *50*, 11739−11742.

(13) Wu, M.; Lin, X.; Wang, Y.; Wang, L.; Guo, W.; Qi, D.; Peng, X.; Hagfeldt, A.; Gratzel, M.; Ma, T. L. *J. Am. Chem. Soc.* **2012**, *134*, 3419−3428.

(14) Li, G. R.; Wang, F.; Jiang, Q. W.; Gao, X. P.; Shen, W. P. *Angew. Chem., Int. Ed.* **2010**, *49*, 3653−3656.

(15) Sun, H. C.; Qin, D.; Huang, S. Q.; Guo, X. Z.; Li, D. M.; Luo, Y. H.; Meng, Q. B. *Energy Environ. Sci.* **2011**, *4*, 2630−2637.

(16) Wang, M. K.; Alina, M.; Marsan, A. B.; Pootrakulchote, N.; Zakeeruddin, S. M.; Grätzel, M. *J. Am. Chem. Soc.* **2009**, *131*, 15976−15977.

(17) Kung, C. W.; Chen, H. W.; Lin, C. Y.; Huang, K. C.; Vittal, R.; Ho, K. C. *ACS Nano* **2012**, *6*, 7016−7025.

(18) Wu, M. X.; Wang, Y. D.; Lin, X.; Yu, N. S.; Wang, L.; Wang, L. L.; Hagfeldt, A.; Ma, T. L. *Phys. Chem. Chem. Phys.* **2011**, *13*, 19298−19301.

(19) Yang, Y. Y.; Zhu, L. F.; Sun, H. C.; Huang, X. M.; Luo, Y. H.; Li, D. M.; Meng, Q. B. *ACS Appl. Mater. Interfaces* **2012**, *4*, 6162−6168.

(20) Tachan, Z.; Shalom, M.; Hod, I.; Rühle, S.; Tirosh, S.; Zaban, A. *J. Phys. Chem. C* **2011**, *115*, 6162−6166.

(21) Xu, J.; Yang, X.; Yang, Q. D.; Wong, T. L.; Lee, C. S. *J. Phys. Chem. C* **2012**, *116*, 19718−19723.

(22) Zhong, H. Z.; Zhou, Y.; Ye, M. F.; He, Y. J.; Ye, J. P.; He, C.; Yang, C. H.; Li, Y. F. *Chem. Mater.* **2008**, *20*, 6434−6443.

(23) Xu, J.; Lee, C. S.; Tang, Y. B.; Chen, X.; Chen, Z. H.; Zhang, W. J.; Lee, S. T.; Zhang, W. X.; Yang, Z. H. *ACS Nano* **2010**, *4*, 1845−1850.

(24) Zhang, Z. Y.; Zhang, X. Y.; Xu, H. X.; Liu, Z. H.; Pang, S. P.; Zhou, X. H.; Dong, S. M.; Chen, X.; Cui, G. L. *ACS Appl. Mater. Interfaces* **2012**, *4*, 6242−6246.

(25) Nose, K.; Soma, Y.; Omata, T. *Chem. Mater.* **2009**, *21*, 2607−2613.

(26) Alexander, R. U.; Carolin, F.; Chirilă, A.; Marc, R. K.; Weidenkaff, A.; Camelia, N. B.; Grolimund, D.; Yaroslav, E. R.; Ayodhya, N. T. *Prog. Photovoltaics* **2012**, *20*, 526−533.

(27) Kovalenko, M. V.; Scheele, M.; Talapin, D. V. *Science* **2009**, *324*, 1417−1420.

(28) Nag, A.; Kovalenko, M. V.; Lee, J. S.; Liu, W. Y.; Spokoyny, B.; Talapin, D. V. *J. Am. Chem. Soc.* **2011**, *133*, 10612−10620.

(29) Zhang, H. T.; Hu, B.; Sun, L. F.; Hovden, R.; Wise, F. W.; Muller, D. A.; Robinson, R. D. *Nano Lett.* **2011**, *11*, 5356−5361.

(30) Bajpai, R.; Roy, S.; Kumar, P.; Bajpai, P.; Kulshrestha, N.; Rafiee, J.; Koratkar, N.; Misra, D. S. *ACS Appl. Mater. Interfaces* **2011**, *3*, 3884−3889.

(31) Roy-Mayhew, J. D.; Bozym, D. J.; Punckt, C.; Aksay, I. A. *ACS Nano* **2010**, *4*, 6203−6211.

(32) Xu, F.; Sun, L. *Energy Environ. Sci.* **2011**, *4*, 818−841.

(33) Imoto, K.; Takahashi, K.; Yamaguchi, T.; Komura, T.; Nakamura, J. I.; Murata, K. *Sol. Energy Mater. Sol. Cells* **2003**, *79*, 459−469.

(34) Han, J.; Kim, H.; Kim, D. Y.; Jo, S. M.; Jang, S. Y. *ACS Nano* **2010**, *4*, 3503−3509.

(35) Kang, D. Y.; Lee, Y. S.; Cho, C. Y.; Moon, J. H. *Langmuir* **2012**, *28*, 7033−7038.